19th International Conference on
Adaptive Structures and Technologies
October 6-9, 2008
Ascona, Switzerland

Behavioral Model and Experimental Validation for Spool-Packaged Shape Memory Alloy Linear Actuators

John A. Redmond[1]*, Diann Brei[1], Jonathan Luntz[1], Alan L. Browne[2], Nancy L. Johnson[2]
[1] University of Michigan, Mechanical Engineering, 2350 Hayward St., 2250 G.G. Brown,
Ann Arbor, MI 48109-2125, USA, (734)764-9156, jredmond@umich.edu
[2] General Motors R&D, MC 480-106-256, 30500 Mound Rd., Warren, MI 48090-9055, USA

ABSTRACT

Shape memory alloy actuators are attractive for many industries because of their high energy density and moderate strokes and forces, which can enable low cost, light weight, high performance devices. SMA wire actuators are particularly advantageous because of their simple form, well-developed manufacturing and quality control, actuation with simple electrical circuits, and faster heating and cooling rates. Unfortunately, packaging the long lengths of SMA wire needed to produce required deflections in many applications is an ongoing technical challenge. This paper investigates spooling as a packaging approach to provide more compact actuator footprints and explores the accompanying design tradeoff between packaging and performance. A predictive analytical model is derived that relates the linear output motion to key design parameters (geometric and frictional properties, SMA material properties, and externally applied loads) within model limits originating from binding due to accumulation of friction across the spool. An experimental study is presented which exercises the model with respect to applied load, wrap angle and spool position within the actuator system, and the results correlate well with the model prediction in both form and magnitude. The study provides insight into the impact of key design parameters and exposes the design tradeoff between the packaging approach and performance losses. Based on the resulting spooling model, actuators can be designed with minimized losses and improved packaging footprints, positioning SMA wire actuators as a viable alternative to conventional industrial actuators.

Keywords: Shape memory alloy, actuator, packaging, spool, spooling model.

1. INTRODUCTION

Shape memory alloy wire actuation is a competitive alternative to conventional actuation based on its high energy density, reduced size and weight, robust performance, and simplistic architectures, becoming economically viable for practical, high yield, low cost industrial applications. While many of the technical challenges relating to SMA (e.g., speed, mechanical connections, cyclic performance degradation) are actively being researched and resolved [1-6], packaging SMA wires compactly while maintaining their high performance continues to be an issue. With typical operating strains between 2-8%, SMA actuators can require wires 12 – 50 times longer than the desired stroke if direct actuation is desired.

To package long lengths of wire more compactly, this paper explores a spooling technique that wraps portions of the wire around mandrels to reduce the packaged length. This technique has been successfully utilized in applications such as active latches [2], pedestrian protection [1], vibration suppression in hand-held arms [6], and biomedical applications [7,8], but it does sacrifice some

performance due to accumulating friction between the SMA wire and mandrel. To fully understand the output motion and limitations of this technique, an analytical model for linear spooled SMA actuators is derived relating the actuator stroke to its geometric and frictional parameters, SMA material properties, and the externally applied load. The model captures complexities introduced by the use of an active material that cannot be accounted for with the typical closed-form equations resulting from belt braking models for passive materials and identifies binding due to accumulated friction around the spool, limiting the predicted performance accordingly. An experimental validation study was conducted to study the effects on spooled actuator performance (with motions up to 20 mm) due to key parameters including load (up to 13 N), wrap angle (up to three complete wraps), spool position within the system (10-300 mm from the fixed end of the wire), and limitations of the model due to binding. The results in this paper demonstrate the ability to model the performance of spooled SMA actuators, assess the model's limitations due to frictional binding, and provide a foundation for analytical actuator design for high performance actuation with compact, customizable packaging.

2. SPOOLED PACKAGING ANALYTICAL MODEL

Analytical design of spooled actuators requires models based on an understanding of the friction losses between the mandrel and SMA wire. Typical modeling approaches have estimated efficiency losses empirically [7], assumed that spooled portions of wire do not contribute to overall motion [9], or adapted belt braking equations [10]; but, these models are often too specific with respect to architecture and material properties, fail to account for portions of the wire that gain and lose contact with the mandrel, and do not explore the model or operating limitations. This paper expands upon earlier work by the authors on rotary spooled actuators [11], which have similar basic mechanics but different boundary conditions, relative motions, and variable portions of the wire's length. The analytical model developed in this paper applies to linear spooled actuators, accounts for modeling complexities that arise from the use of an active material, and can support analytical actuator design with minimized losses and customized packaging.

2-1. Packaging architecture and operation

The general actuator architecture for linear spooled actuators (Figure 1) comprises a cylindrical mandrel, an SMA wire, and a single degree-of-freedom sliding constraint on the output motion. The SMA wire has three continuous segments: an input tail fixed to ground and in tangential contact with the mandrel, a wrapped portion in frictional contact with the mandrel, and an output tail in tangential contact with the mandrel and attached to the linear motion output. The packaging architecture is highly customizable since the wire length, wrap angle, and mandrel size can be selected based on the actuator application's needs. Varying the spool position (defined relative to the datum AA perpendicular to the fixed end of the wire) affords further design flexibility.

The actuator's range of motion is defined

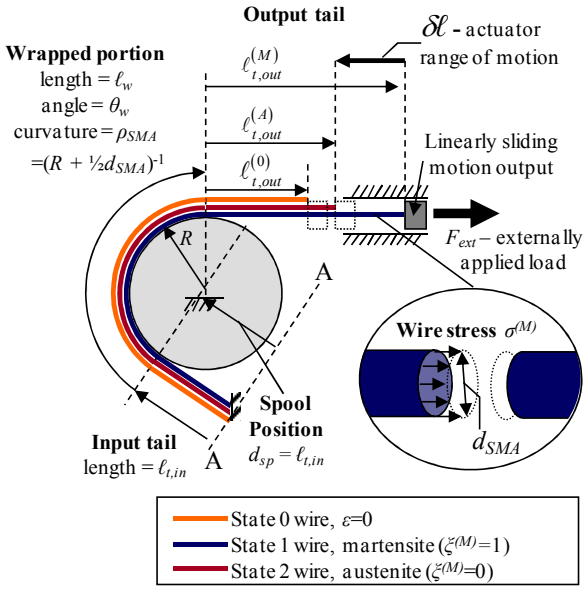

Figure 1. General architecture for spooled SMA actuators. The general architecture for a spooled actuator with a linear motion output is shown with the key operation states.

with respect to three main operation states (Figure 1). All motions, geometries, and strains of the actuator are referenced to *State 0* (the zero strain reference state, orange) which is attained by heating the SMA wire to austenite under no load, and remaining in *State 0* upon cooling assuming no two-way effect. The *State 1* (martensite SMA actuator under an applied load, blue) is achieved by stretching the SMA wire along its length to $\ell_{tot}^{(M)}$, either by applying a load to a martensite *State 0* actuator or by cooling an austenite *State 2* actuator under load . Likewise, the *State 2* (austenite SMA actuator under an applied load, red) is achieved by heating the SMA wire under load which contracts to $\ell_{tot}^{(A)}$. The model assumes unilateral wire motion throughout its operation such that in *State 1* the entire wire lengthens from the previous state, and in *State 2* the entire wire contracts from the previous state such that all friction loads act in the same direction in a particular state. The actuator moves through its range of motion $\delta\ell$ via cyclic heating and cooling where $\delta\ell$ is the difference between the martensite and austenite wire lengths: $\delta\ell = \ell_{tot}^{(M)} - \ell_{tot}^{(A)} = \ell_{t,out}^{(M)} - \ell_{t,out}^{(A)}$.

2-2. Derivation of actuator motion

The motion of the actuator results in deformation due to the changing strain between the operational states. Each state is modeled to consider losses due to friction and the stress and strain variations along the wire with respect to the modeling parameters and applied load. The model assumes Coulomb friction and unilateral extension or contraction of the wire, and the resulting tensile, normal, and friction loads on a differential element of wire in contact with the spool are diagrammed in Figure 2. The motion and loads of the *State 2* austenite actuator are similar to those of the *State 1* actuator, except that wire contracts rather than extends such that the friction forces are in the opposite direction.

From the free body diagram, the sum of forces in the radial direction ΣF_r and the sum of moments about the spool's center ΣM_0 are

$$\Sigma F_r = N - \left(2F_{SMA} + dF_{SMA}\right)\sin\left(\tfrac{1}{2}\theta\right) = 0\,, \qquad \text{and} \qquad \Sigma M_0 = \frac{\left(dF_{SMA} \pm \mu N\right)}{\rho_{SMA}} = 0 \tag{1,2}$$

where N is the normal reaction force, F_{SMA} is the wire tension, and μ is the coefficient of friction between the spool and wire. Combining the force and moment equations (Eq. 1,2) and assuming that the second order term $dF_{SMA}d\theta$ is negligible, the normal force N cancels yielding

$$\pm\mu d\theta = \frac{dF_{SMA}}{F_{SMA}}\,. \tag{3}$$

To determine the stress and strain at intermediate points along the spool, the expression relating the changing tension due to friction (Eq. 3) is integrated from a general point θ on the spool ($0 < \theta < \theta_w$) to the upper limit θ_w at the output where the applied tension is known. Dividing by the SMA cross-sectional area (A_{SMA}) gives stress as a function of position,

$$\sigma^{(M)}\{\theta\} = \sigma_{ext}e^{\mu(\theta-\theta_w)},\ \sigma^{(A)}\{\theta\} = \sigma_{ext}e^{-\mu(\theta-\theta_w)} \tag{4,5}$$

where $\sigma^{(M)}$ is the State 1 stress, $\sigma^{(A)}$ is the State 2 stress, and σ_{ext} is the output tail stress ($\theta=\theta_w$) resulting from the applied load F_{ext}.

The model is based on a generalized form of the constitutive law allowing for varying levels of

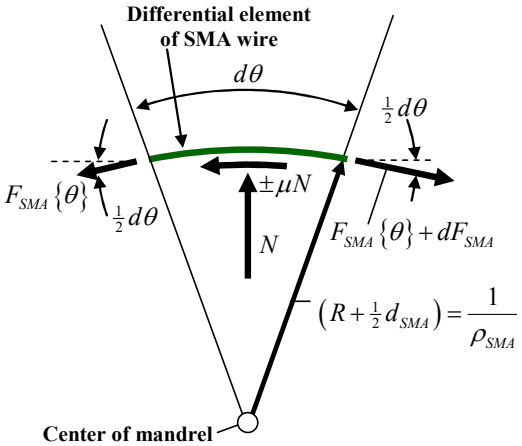

Figure 2. Free body diagram of a differential element of SMA in sliding contact with the spool. In *State 1* (martensite), the wire extends producing counterclockwise friction. In *State 2* (austenite), the wire contracts, producing clockwise friction.

simplicity and accuracy. Two simplified functions represent the strain based on constitutive laws for the fully martensite *State 1* ($f_{SMA}^{(M)}$) and fully austenite *State 2 (* $f_{SMA}^{(A)}$):

$$\varepsilon^{(M)}\{\theta\} = f_{SMA}^{(M)}\left\{\sigma\{\theta\}\right\}, \quad \text{and} \quad \varepsilon^{(A)}\{\theta\} = f_{SMA}^{(A)}\left\{\sigma\{\theta\}\right\}. \tag{6,7}$$

Based on the stress functions (Eq. 4,5) and the generalized strain functions (Eq. 6,7), the martensite and austenite strains as functions of position are

$$\varepsilon^{(M)}\{\theta\} = f_{SMA}^{(M)}\left\{\sigma_{ext}e^{\mu(\theta-\theta_w)}\right\}, \quad \text{and} \quad \varepsilon^{(A)}\{\theta\} = f_{SMA}^{(A)}\left\{\sigma_{ext}e^{-\mu(\theta-\theta_w)}\right\}. \tag{8,9}$$

As the wire deforms between states, portions of the wire gain or lose contact with the spool. To account for all portions of the wire in determining its deformed length, compatibility equations relate the *State 0* reference length ($\ell_{tot}^{(0)}$) to the deformed State *1* and *State 2* lengths ($\ell_{tot}^{(M)}$ and $\ell_{tot}^{(A)}$) based on the strain functions (Eq. 8,9). For a differential element of State 1 wire, the definition of strain ($\varepsilon^{(M)} = (ds^{(M)} - ds^{(0)})/ds^{(0)}$) is solved for $ds^{(0)}$ and integrated along the wire's length to give

$$\int_0^{\ell_{tot}^{(0)}} ds^{(0)} = \int_0^{\ell_{tot}^{(M)}} \left(1+\varepsilon^{(M)}\right)^{-1} ds^{(M)}. \tag{10}$$

Expanding the right hand side of the equation into three integrals for the input tail, wrapped portion, and output tail, the *State 0* wire length (Eq. 10) becomes

$$\ell_{tot}^{(0)} = \underbrace{\int_0^{\ell_{t,in}} \left[1+\varepsilon^{(M)}\{\theta=0\}\right]^{-1} ds^{(M)}}_{\text{input tail}} + \underbrace{\int_0^{\theta_w/\rho_{SMA}} \left[1+\varepsilon^{(M)}\left\{\theta=\rho_{SMA}ds^{(M)}\right\}\right]^{-1} ds^{(M)}}_{\text{wrapped portion}} + \underbrace{\int_0^{\ell_{t,out}^{(M)}} \left[1+\varepsilon^{(M)}\{\theta=\theta_w\}\right]^{-1} ds^{(M)}}_{\text{output tail}} \tag{11}$$

With constant strains in both tails, the expression is simplified and solved for the unknown deformed *State 1* length ($\ell_{tot}^{(M)}$), and a similar derivation yields the State 2 length ($\ell_{tot}^{(A)}$), such that

$$\ell_{tot}^{(M)} = \ell_w + \ell_{t,in} + \left(\ell_{tot}^{(0)} - \frac{\ell_{t,in}}{1+f_{SMA}^{(M)}\left\{\sigma_{ext}e^{-\mu\theta_w}\right\}} - \int_0^{\theta_w/\rho_{SMA}} \left[1+\varepsilon^{(M)}\left\{\theta=\rho_{SMA}ds^{(M)}\right\}\right]^{-1} ds^{(M)}\right)\left(1+f_{SMA}^{(M)}\{\sigma_{ext}\}\right) \tag{12}$$

$$\ell_{tot}^{(A)} = \ell_w + \ell_{t,in} + \left(\ell_{tot}^{(0)} - \frac{\ell_{t,in}}{1+f_{SMA}^{(A)}\left\{\sigma_{ext}e^{\mu\theta_w}\right\}} - \int_0^{\theta_w/\rho_{SMA}} \left[1+\varepsilon^{(A)}\left\{\theta=\rho_{SMA}ds^{(A)}\right\}\right]^{-1} ds^{(A)}\right)\left(1+f_{SMA}^{(A)}\{\sigma_{ext}\}\right) \tag{13}$$

The actuator motion is the difference between the *State 1* and *State 2* lengths: $\delta\ell = \ell_{tot}^{(M)} - \ell_{tot}^{(A)}$.

2-3. Limitations on model

For larger wrap angles, accumulated friction can cause the SMA wire to bind to the mandrel, which occurs when the unilateral motion assumption is violated. At the input tail ($\theta=0$), increasing the wrap angle causes the strain in the *State 1* martensite wire to decrease (Eq. 8) and the strain in *State 2* austenite wire to increase (Eq. 9), causing the input tail strains in each state to approach one another until the critical binding angle θ_B is reached where the strains are equal for the condition

$$\theta_B = \theta_w^{(0)} \Leftrightarrow \varepsilon^{(M)}\{\theta=0\} = \varepsilon^{(A)}\{\theta=0\}. \tag{14}$$

Since no relative motion occurs between the wire and mandrel at the binding point, wrapping beyond the binding angle will produce no further actuator motion. Thus, motions for actuators that bind ($\theta_w > \theta_B$) are predicted to be the same as actuators with wrap angles equal to θ_B.

3. EXPERIMENTAL STUDY

To validate the analytical model and gain insight into the effect of key parameters that relate to performance, packaging, and binding, an experimental study was conducted. To reduce variation in SMA properties over cycles, the wire was shaken down prior to testing by heating and cooling the unspooled wire under a 45 N load with a 6.5% maximum strain constraint until the motion stabilized according to the procedure defined by Sun et al. [12]. The measured stress-strain behavior was approximated with a linear fit for the austenite phase and a third-order polynomial for the martensite phase (Figure 3). To further ensure consistent wire performance, curves were re-generated periodically throughout the spooling study.

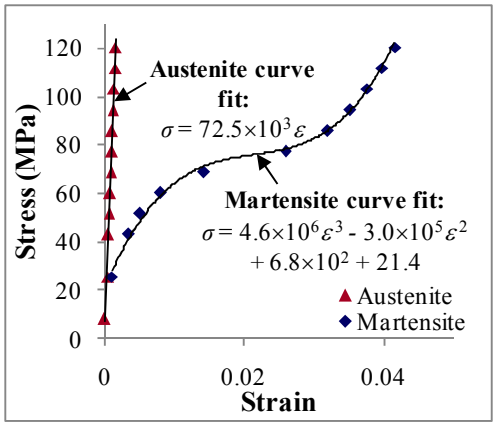

Figure 3. Simplified stress-strain model compared to data for a typical SMA wire.

In a typical test, the SMA wire and mandrel were installed in the experimental test apparatus (Figure 4) varying the applied load, wrap angle, and spool position configuration in each test. Electrical current was applied to the wire (regulated and monitored by LabView software and a laptop computer equipped with data acquisition hardware) to resistively heat it until a steady state position for austenite (1.8 A for about 30 seconds) was reached. The current was removed and the wire was allowed to cool to ambient temperature reaching its steady state position for martensite (0A for about 3 minutes). Each trial was repeated 3 – 5 times to ensure consistency andz repeatability. For each test the actuator linear range of motion was measured by a laser displacement probe, loads were applied with known weights, and wire tension was measured by a load cell at the fixed end of the input tail. The average coefficient of friction was estimated to be between 0.1 and 0.125 based on load cell measurements, known applied loads, and the Capstan equation [13]. Laboratory temperature was regulated between 19 - 21°C. The experimental study tested three aspects of the spooling model – applied load, wrap angle, and spool position– testing its accuracy and its range and providing insights into the behavior of spooled actuators and the related design issues.

3-1. Effect of applied load

For the applied load experiments, a single length of wire (450 mm) was tested with a 10 mm input tail and varying wrap angles for different binding cases: 0 wraps provided the baseline case for no spooling, 1 wrap with no binding predicted, 2 wraps on the borderline of the binding prediction, and 3 wraps with binding predicted to occur. At each wrap angle, the applied load was varied between 0 and 13 N. The data matches the model well in shape and magnitude with the characteristic shape of the martensite plateau evident in the data (Figure 5). For the expected range of friction coefficients (μ=.1-.125) errors were small with 3.4%-16.5% average error for the spooled actuators and increasing errors for larger amounts of wrapping. The characteristic inflection in the applied load

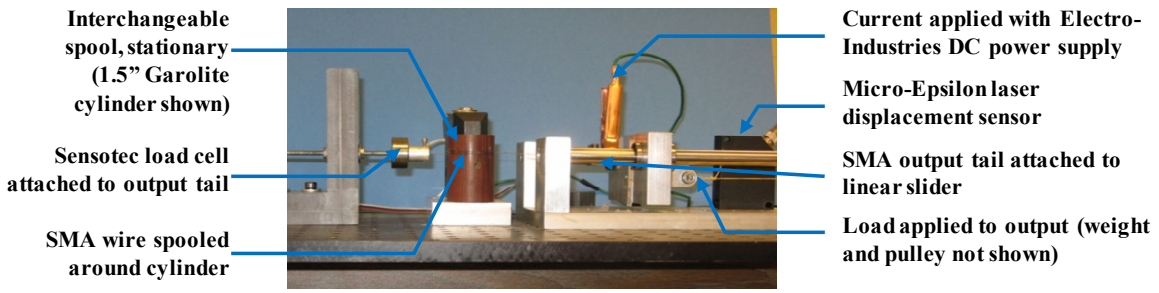

Figure 4. Experimental apparatus for linear spooled actuator experiments. The configuration shown uses a spooled SMA wire with 0.38 mm diameter, and 3 wraps shown around a 38 mm diameter mandrel. The sliding motion output constrains the motion to a linear single degree of freedom, and is also the attachment point for the applied load F_{ext}.

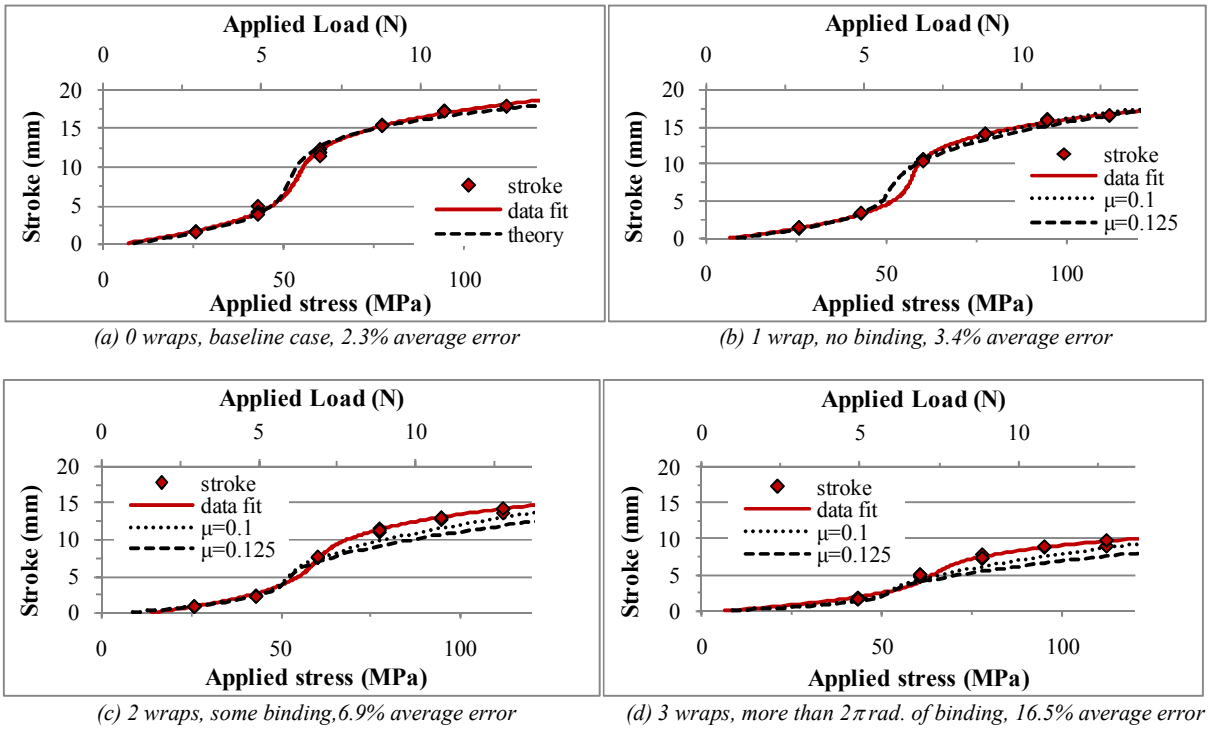

(a) 0 wraps, baseline case, 2.3% average error

(b) 1 wrap, no binding, 3.4% average error

(c) 2 wraps, some binding,6.9% average error

(d) 3 wraps, more than 2π rad. of binding, 16.5% average error

Figure 5. Effect of applied load experimental results. Data represents the actuator's range of motion as it is thermally cycled between austenite and martensite states for a SMA wire across a range of applied loads and number of wraps.

curves results from the martensite plateau. Wrapping the wire distributes the stress and strain of the wire along the martensite and austenite curves, which is reflected by the stroke vs. load becoming more distorted and the motion losses becoming more pronounced as more wire is wrapped around the mandrel.

3-2. Effect of wrap angle

For the wrap angle experiments, a single length of wire (450 mm) with a constant input tail length (10 mm) was used. The amount of wire wrapped around the mandrel was varied between 0-3 wraps, and experiments were performed at three applied loads to evaluate the effect of the wrapped length for different stress and strain distributions on the wire. The actuator stroke as a function of length is shown in Figure 6a. Subtracting the theoretical contribution to motion due to the tail portions of the SMA wire, the spooled portion's contribution to overall motion is plotted in Figure 6b.

The data correlates well with theory with a 3.4 – 5.4% average error for the overall stroke.

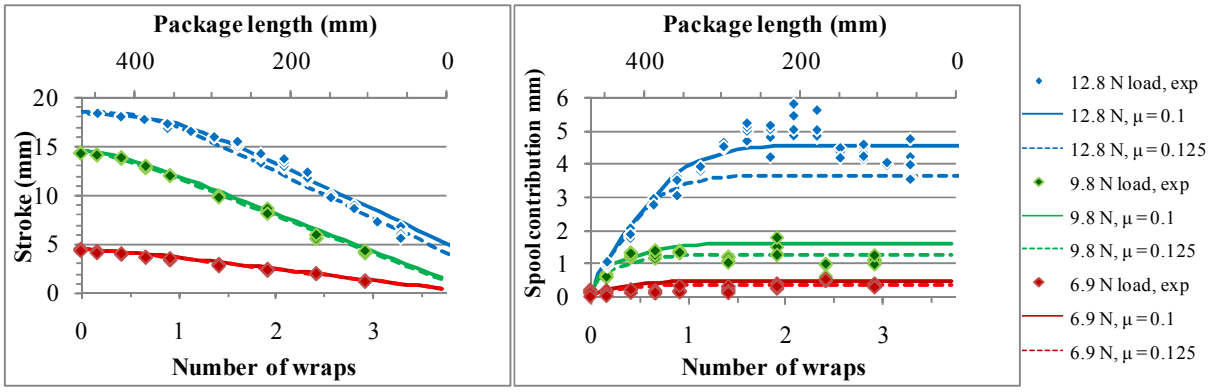

(a) Effect of packaging on stroke

(b) Spooled portion's contribution to stroke

Figure 6. Effect of wrap angle on overall motion experimental results. Varying the wrap angle on a constant length SMA wire, the measured stroke is shown, along with the contribution due to the spooled portion of the wire.

Since the effect of spooling builds up as more wire is wrapped around the mandrel, the decline in the motion with wrapped length is initially low and becomes steep in slope until the binding condition is met, at which point the slope becomes constant and the stroke drops of linearly as wrap angle increases. The spooled portion's contribution to stroke agrees with 3.8-17.5% average error for the non-binding cases and increases to 9.4-23% average error for configurations with binding. The initial increase and leveling off of the spooled portion's contribution to stroke is due to binding, which supports the hypothesis that the binding portions of the wire do not contribute to the overall stroke. The results also demonstrate a distinct tradeoff between performance and packaging with the largest strokes resulting from the largest package lengths. Additionally, the spooled portion's contribution to stroke levels off once binding occurs, which indicates that binding configurations should be avoided in design since there is no benefit to performance for the additional cost of wrapping more SMA wire.

3-3. Effect of spool position

To test the effect of moving the spool along its length, a constant length (450 mm) of wire was tested and the spool's position (d_{sp}=$\ell_{t,in}$) with respect to the input end was varied, and expressed quantitatively in terms of the input tail length. The predicted motion was experimentally validated for 1, 2, and 3 wraps of SMA wire around the mandrel, testing the non-binding, borderline binding, and binding cases (Figure 7). The model predicts that the actuator stroke decreases linearly by increasing the input tail length since it decreases the length of the output tail, which is not subject to motion losses due to spooling and can make a greater contribution to the actuator's overall motion per unit length. Thus, the most advantageous placement of the spool is nearest to the fixed input where the output tail is largest. The linear trend was validated in the experiments with 3.9 – 6.9% average error on the stroke prediction for the non-binding case (1 wrap) and 3.7-35% error for the binding cases. Additionally, the slope of the data is within the expected range for the non-binding case, but the binding cases demonstrated error between 15-21% for the binding cases with the model consistently under-predicting the motion. The additional motion comes from stick-slip motion, a less predictable and less consistent behavior that results from friction building up and then suddenly relaxing as the wire slips along the mandrel. The study of spool position also demonstrates that the actuator motion becomes increasingly sensitive to the position of the spool for larger amounts of wrapping with the stroke maximized by having the largest output tail possible. When packaging is an issue and the spool cannot be positioned at the input end, it is advantageous to position as closely to the input as possible with the spool position becoming more critical for larger wrap angles.

4. CONCLUSION

SMA actuators are attractive alternatives to conventional actuators from energy density, cost, and weight perspectives, but have been limited by difficulty in packaging long lengths of wire within a compact actuator footprint. This paper introduced a spooling technique that can overcome the barriers to packaging SMA wire to enable compact, high performance actuation for a wide variety of applications. The analytical model relates the linear output motion to key design parameters (actuator geometric and frictional properties, SMA material properties, and externally applied loads) within model limits originating from binding due to

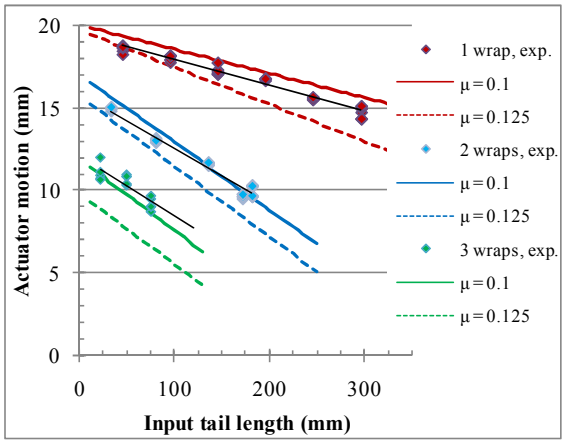

Figure 7. Effect of spool position experimental results. Experiments were run for a range of input tail lengths varying the position of the mandrel with respect to the fixed end of the SMA wire and compared to the theoretical prediction for the expected range of friction.

accumulation of friction across the spool. The model builds on similar mechanics as those in belt-braking models, but takes additional steps to account for the non-linear, phase and stress dependent properties of the active material by predicting the strain gradient and wire deformation that result from spooling. The experimental study demonstrated the model's accuracy with respect to three main variables – applied load, wrap angle, and spool position – and correlated very well with theory in both form and magnitude, especially for the non-binding range of actuator designs (3.4 - 17% error) where the assumption of unilateral motion is satisfied. When the unilateral motion assumption was violated, binding behavior occurred, preventing portions of the SMA wire from slipping on the mandrel. The study demonstrated that increasing the applied load increases the actuator stroke non-linearly, that increasing wrap angle can reduce overall package size with a tradeoff of reduced performance and an upper limit on the amount of packaging due to binding, and that the spool's position from the fixed end and the actuator motion are linearly related with the most advantageous placement of the spool nearest to the fixed input end of the SMA wire. Based on the results of this study, spooled packaging techniques and the accompanying predictive model can provide a useful foundation for analytical actuator design for synthesizing high performance actuators with compact packaging and minimized losses. With spooling techniques to overcome packaging challenges, SMA can create expanded opportunities for improving actuator cost, weight, and energy density to bring the numerous practical advantages of SMA to a broader application space.

REFERENCES

1. Barnes, B., Brei, D., Luntz, J., Browne, A., and Strom, K. "Panel Deployment Using Ultrafast SMA Latches", Proc. ASME, IMECE2006-15026 (2006).
2. Redmond, J. A., Brei, D. E., Luntz, J., Browne, A. L., Johnson, N. L., and Strom, K. "Design and Experimental Validation of an Ultrafast SMART (Shape Memory Alloy ReseTtable) Latch", Proc. ASME, IMECE2007-43372 (2007).
3. Webb, G., Wilson, L., Lagoudas, D., and Rediniotis, O. "Control of SMA actuators in dynamic environments", Proc. SPIE 3667, 278-289 (1999).
4. Grummon, D. S., Shaw, J. A., and Foltz, J. "Fabrication of cellular shape memory alloy materials by reactive eutectic brazing using niobium", Mater. Sci. Eng. A, 438-440, 1113-1118 (2006).
5. Erbstoeszer, B., Armstrong, B., Taya, M., and Inoue, K. "Stabilization of the shape memory effect in NiTi: an experimental investigation", Scr. Mater. 42, 1145-1150 (2000).
6. Pathak, A., Brei, D., Luntz, J., LaVigna, C., and Kwatny, H. "Design and quasi-static characterization of SMASH: SMA stabilizing handgrip", Proc. SPIE 6523 (2007).
7. Wang, G. and Shahinpoor, M. "Design of a knee and leg muscle exerciser for paraplegics using a shape memory alloy rotary joint actuator", Proc. SPIE 3324, 193-201 (1998).
8. Menciassi, A., Gorini, S., Moglia, A., Pernorio, G., Stefanini, C., and Dario, P. "Clamping Tools of a Capsule for Monitoring the Gastrointestinal Tract Problem Analysis and Preliminary Technological Activity." Proc. IEEE, Robotics and Automation, 1309-1314 (2005).
9. Tanaka, K. "A Thermomechanical Sketch of Shape Memory Effect: One-Dimensional Tensile Behavior", Res. Mech. 18, 251-263 (1986).
10. Huang, W. "Modified Shape Memory Alloy (SMA) model for SMA wire based actuator design", J. Intell. Mater. Syst. Struct. 10, 221-231 (2000).
11. Redmond, J., Brei, D., Luntz, J., Browne, A., Johnson, N. "Behavioral model and experimental validation for a spool-packaged shape memory alloy actuator,", Proc. SPIE 6930 (2008).
12. Sun, X., Pathak, A., Luntz, D., Brei, D., Alexander, P., Johnson, N. "Stabilizing SMA actuator performance through cyclic shakedown: an empirical study," Proc. SPIE 6930 (2008).
13. Howell, H. "The general case of friction of a string round a cylinder," J. Textile Inst., v44(8/9), t359-362 (1953).